Polymer-Based Catch-Bonds

Polymer-Based Catch-Bonds

Hsieh Chen and Alfredo Alexander-Katz*
Department of Materials Science and Engineering, Massachusetts Institute of Technology, Cambridge, Massachusetts

ABSTRACT Catch-bonds refer to the counterintuitive notion that the average lifetime of a bond has a maximum at a nonzero applied force. They have been found in several ligand-receptor pairs and their origin is still a topic of debate. Here, we use coarse-grained simulations and kinetic theory to demonstrate that a multimeric protein, with self-interacting domain pairs, can display catch-bond behavior. Our model is motivated by one of the largest proteins in the human body, the von Willebrand Factor, which has been found to display this behavior. In particular, our model polymer consists of a series of repeating units that self-interact with their nearest neighbors along the chain. Each of the units mimics a domain of the protein. Apart from the short-range specific interaction, we also include a linker chain that will hold the domains together if unbinding occurs. This linker molecule represents the sequence of unfolded amino acids that connect contiguous domains, as is typically found in multidomain proteins. The units also interact with an immobilized ligand, but the interaction is masked by the presence of the self-interacting neighbor along the chain. Our results show that this model displays all the features of catch-bonds because the average lifetime of a binding event between the polymer and the immobilized receptor has a maximum at a nonzero pulling force of the polymer. The effects of the energy barriers for detaching the masking domain and the ligand from the binding domain, as well as the effects of the properties of the polypeptide chain connecting the contiguous domains, are also studied. Our study suggests that multimeric proteins can engage in catch-bonds if their self-interactions are carefully tuned, and this mechanism presumably plays a major role in the mechanics of extracellular proteins that share a multidomain character. Furthermore, our biomimetic design clearly shows how one could build and tune macromolecules that exhibit catch-bond characteristics.

INTRODUCTION

Biological bonds usually contain receptors and their complementary ligands, and dissociate readily when force is applied. However, in recent years there has been growing interest in catch-bonds, which refers to the counterintuitive phenomenon that the average bond lifetime increases when external force is applied to the system. Several naturally occurring receptor-ligand pairs have been observed to display catch-bond behavior experimentally, and it is believed that many more have this property as well (1). For example, the type 1 fimbrial adhesive protein/mannose pair (2), P-selectin/P-selectin-glycoprotein-ligand-1 (PSGL-1) (3), L-selectin/PSGL-1 (4), actin/myosin (5), von Willebrand factor (vWF)/glycoprotein Ibα (GPIbα) (6), and integrin/fibronectin (7) display catch-bond behavior. Experiments (2,6,8–11) and simulations (2,6,8,9,12,13) have been held to unveil the mystery behind the catch-bonds, and there have been two mechanisms proposed—allosteric (2,9–11) and sliding-rebinding (6,8,12,13). Each mechanism has its own advantages, but concrete evidences to support which is the correct one are still under way.

Theoretical models have been formulated, and can be broadly classified into a two-pathway model (14–18), a force-induced deformation model (19,20), a dynamic disorder model (21,22), or an entropic-elasticity model (23). Each model successfully describes the experimental data, yet there is no universal agreement. Current research has thus tended to focus more on the specific atomic level details inside the protein structures that lead to this behavior, to unravel which is the correct mechanism. Steered molecular dynamics simulations (2,6,8,9,12,13) have usually been employed to capture the force effects on the catch-bond behavior. Due to the computation limit, steered molecular dynamics simulations can only be performed around the nanosecond timescales, and using forces of one to two orders of magnitude higher than general conditions.

In this study, we use coarse-grained Brownian dynamics simulations to demonstrate that catch-bond behavior can also be achieved from an alternative model in which all the atomic details are effectively taken into account in the binding-unbinding rate constants between domains of a protein and the polymer nature of the multimeric protein that effectively regulates the binding behavior. Thus, our model is a mesoscopic model that includes the atomistic details in an effective way. The motivation for this model comes from the observation of a multimeric protein, von Willebrand factor (vWF), which displays catch-bond behavior. vWF plays an essential role in the initial stages of blood clotting by mediating the adhesion of platelets to the injured vessels. Each subunit of vWF contains multiple copies of A, B, C, and D type domains that are arranged in the order (24) D′-D3-A1-A2-A3-D4-B1-B2-B3-C1-C2-CK. The A1 domain of the protein contains the binding site for platelet glycoprotein GPIbα, and has displayed a catch-bond character (6).

Submitted December 21, 2009, and accepted for publication November 16, 2010.

*Correspondence: aalexand@mit.edu

Editor: R. Dean Astumian.

0006-3495/11/01/0174/9 $2.00

doi: 10.1016/j.bpj.2010.11.023

However, it has recently been shown that the A2 domain interferes with the GPIbα-binding conformation in the A1 domain, blocking GPIbα-mediated platelet adhesion (25). Here we hypothesize that the A2 domain acts as a masking domain to the A1 binding site under regular nonstressed conditions. Under load, however, the masking domain can become detached from the binding domain, exposing the binding site of the protein to its complementary ligand that in turn increases the average interaction lifetime of the bond. Apart from vWF, we believe that fibronectin is another example where the multidomain structure of the protein can lead to stress stiffening of fibronectin networks due to the appearance of the aforementioned effect. To our knowledge, this is the first time that a model is being put forward that explains the stress-enhanced bonding of multimeric proteins. Furthermore, our design could be a generic route for creating biomimetic polymer-based catch-binding molecules.

MODEL AND SIMULATION METHODS

The self-interacting domains of a multimeric protein are considered explicitly, and we focus simply on a dimer consisting of two beads of radius a connected with a finitely extensible nonlinear elastic (FENE) springs (26), which represents the polypeptide chain connecting the domains, in a three-dimensional simulation box. FENE springs, along with the worm-like chain springs (27), are popular nonlinear springs for describing (bio) polymers with rigid chains (28,29). The potential energy of the FENE spring is given by

$$U_{FENE}(R) = -\frac{kR_0^2}{2}\ln\left[1-\left(\frac{R}{R_0}\right)^2\right], \qquad (1)$$

where k is the spring constant, R is the bond length, and R_0 is the maximum bond extension. Other parts on the protein are simulated implicitly by equivalent forces and potentials. When moving in flow, each monomer of the polymer chain feels three forces: the spring force connecting the monomer to the next monomer; the spring force to the previous monomer; and the fluid drag force, which is proportional to the velocity difference of the monomer and the fluid. The fluid velocity gradient in shear flow will generate a force gradient along the polymer chain when the chain is tipped at an angle with respect to the flow direction, and this is the origin of polymer stretching. In fact, during the last few decades it has been shown that polymers in shear-flow exhibit periodic elongation, relaxation, and tumbling behavior (30–33). In good solvent conditions, the unfolding-refolding transition can occur for very small shear rates (31). In bad solvent condition, however, the transition only occurs above a critical shear rate (33). Here we only consider the stretched conformation that has been shown to be the active conformation of vWF. Fig. 1 *A* shows a sketch of the flow chamber of our simulation. A multidomain protein (a single chain polymer, which is represented by *green beads*) moves with the shear flow, while the ligand (represented by a *gray bead*) is fixed on the bottom of the chamber. As mentioned before, we are only interested in the events where the protein is in the elongated state when passing the ligand. We further assume that the relaxation time of the elongated protein is long enough that the protein is always in the stretched state during the protein-ligand interaction. Fig. 1 *B* shows some possible trajectories for the protein; however, we only consider the case that the trajectory of the protein is coincident with the ligand.

Fig. 2 shows a schematic force analysis of the dimer in shear flow in the stretched state (seen from the center of mass of the dimer). By defining an effective drag force that contains the effect of the rest of the chain, one can then just work with two beads, and the effective friction coefficient of the beads is related to the length of the polymer being dragged behind, as well as the tilt angle. The overall force on each of the beads is zero, which means that the tension between the dimer equals to the effective drag force ($f_{tension} = f_{drag}$), and the tension force should be proportional to the shear flow rate. Also, when the chain becomes longer, it can be

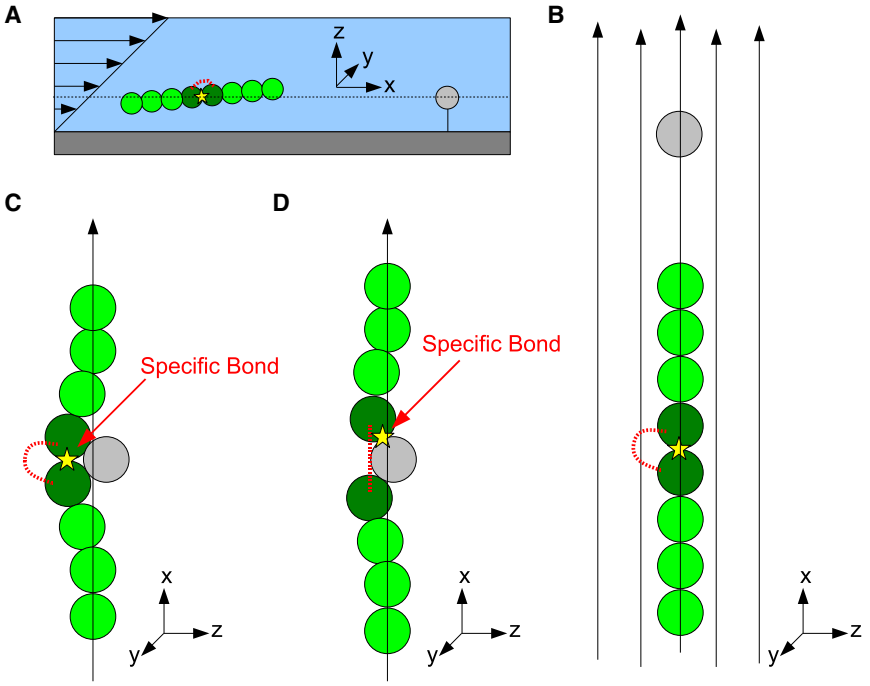

FIGURE 1 (*A*) Schematic of the flow chamber in our simulation. (*B*) Possible trajectories of the protein when moving in flow. (*C*) The masking domain is attached to the binding domain when the protein passes the ligand. The bond is denoted by a yellow star. (*D*) The masking domain is detached from the binding domain, and the binding domain forms a specific bond (*yellow star*) to the ligand. (Note that the protein length in this figure is arbitrary, and in most cases, the protein length is much longer than shown.)

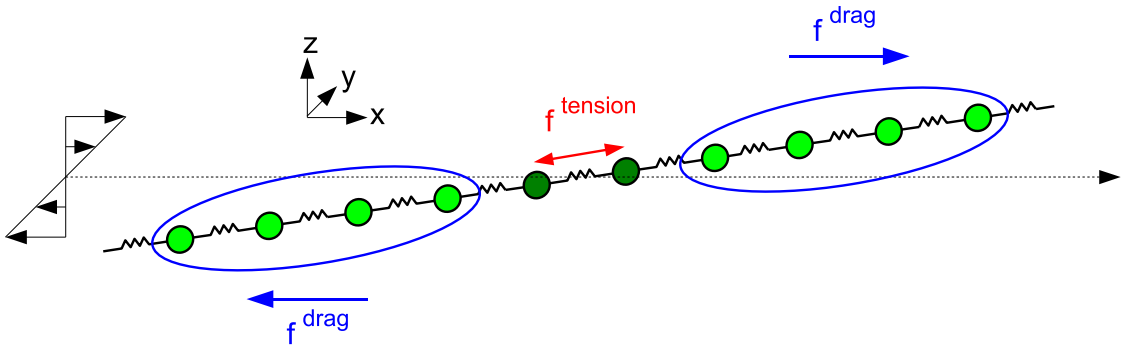

FIGURE 2 Force analysis of the dimer in shear flow in the stretched state (seen from the center of mass of the dimer). Each monomer feels an effective drag force, as well as the tension between the dimer.

shown that the monomers on the chain are constrained from deviating-away from the moving trajectory. Fig. 3 *A* shows the bead and spring model of an unperturbed long chain polymer (which is stretched and moves in $+x$ direction). Without perturbations, the monomers are aligned along the chain. Fig. 3 *B* shows the same polymer when passing an obstacle. In practice, we assume that the polymer (protein) length is much longer than the size of the obstacle (ligand). Because the obstacle only perturbs a small portion of the chain, other parts of the chain are, in essence, unaffected. The tension along the chain tends to bring the perturbed monomers back to the central axis, and this is modeled through a harmonic soft potential. The ligand is also modeled by a bead of radius a. Different from the free-moving dimer, however, the ligand bead is fixed in space. A Lennard-Jones (LJ) potential,

$$U_{LJ} = \varepsilon \sum_{i,j} \left[\left(\frac{2a}{r_{i,j}} \right)^{12} - 2 \left(\frac{2a}{r_{i,j}} \right)^{6} \right], \tag{2}$$

where ε is the depth of the potential and $r_{i,j}$ is the distance between the i^{th} and the j^{th} bead, is used to represent the generalized nonspecific secondary interactions among the biomolecules. These nonspecific interactions may include hydrophobic forces, van der Waals forces, or weak hydrogen bonds.

The front bead of the dimer (which is defined as the binding domain in our simulation) is a receptor capable to form specific bonds with the rear bead (which is defined as the masking domain) or the ligand, but not with both at the same time. When the receptor domain is not bonded, we allow it to form bonds with either the ligand or the masking domain if the distance between them is less than the reaction radius, $R_{reaction}$ = bond length $(2a) + 5\%$ bond length set to $0.1a$. The probability of forming a bond is given by

$$P_{attach} = \exp\left(-\frac{E_{attach}}{k_B T} \right), \tag{3}$$

where E_{attach} is the energy barrier for the two interacting beads to form a bond, k_B is the Boltzmann constant, and T is the temperature. When forming specific bonds, biomolecules usually need to perform particular molecular structures to fit into each other, and this effect is modeled through an energy barrier of attachment in our coarse-grained model. When a bond is formed, a stiff spring, which is represented by a harmonic spring with constant $k_{bond} = 100\ k_B T/a^2$ and equilibrium bond length $2a$, is placed between the receptor and masking domain (or the ligand). To break the bond, the Bell mechanism (34) is used. Despite the energy barrier of detachment, E_{detach}, the lifetime of the bond also depends on the force loaded on the bond f_{bond} and the characteristic bond length r_0. The probability of detachment is given by

$$P_{detach} = \exp\left(-\frac{E_{detach} - r_0 f_{bond}}{k_B T} \right). \tag{4}$$

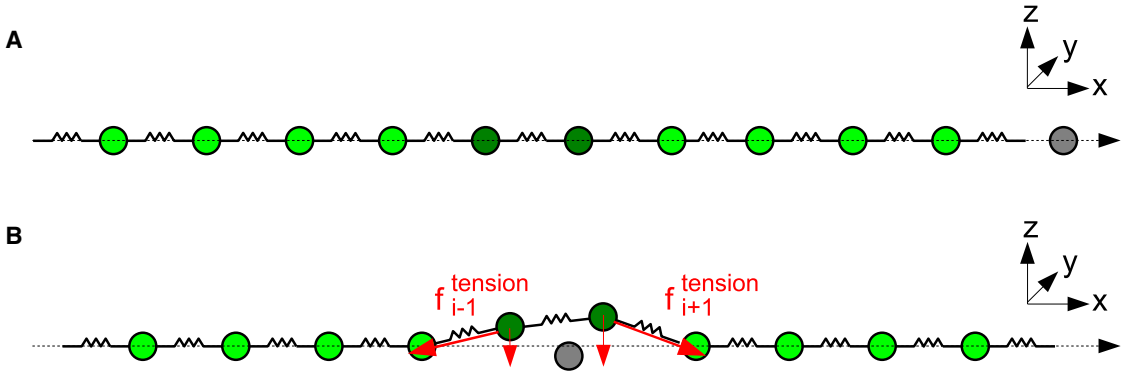

FIGURE 3 Bead and spring model of a stretched long chain polymer. (*A*) When not perturbed, the monomers are aligned along the chain. (*B*) When perturbed in the middle of the chain, the tension along the chain tends to straighten the perturbed parts. This leads to a force directed toward the axis of the polymer, which in our case is modeled by a weak harmonic spring.

The dynamics of bead i with position $\mathbf{r}_i$ is given by the Langevin equation

$$\frac{\partial}{\partial t}\mathbf{r}_i = -\mu\nabla U + \mu\mathbf{f}_i + \xi_i(t), \quad (5)$$

where μ is the mobility of the monomers (or beads), U is the combination of the Lennard-Jones potential, FENE is the spring potential and other implicit potentials, $\mathbf{f}_i$ is the representative external force, and $\xi_i(t)$ is a random velocity that satisfies $\langle\xi_i(t),\xi_j(t')\rangle = 6\,k_BT\mu\delta(r_i - r_j)\delta(t - t')$. To simulate the dynamics of the dimer, we discretized Eq. 5 using a time step $\Delta t = 10^{-5}\tau$, where τ is the characteristic monomer diffusion time $\tau = a^2/\mu k_BT$.

In the beginning of the simulation, the masking domain is attached to the binding domain, and approaches the ligand from behind along the shear flow direction (as shown in Fig. 1 *A*). When the dimer passes the ligand, the masking domain may still be attached to the binding domain, or the masking domain may have been detached during the traveling from the initial position. If the masking domain is attached to the binding domain (that is, the binding domain is masked), the protein can only interact with the ligand with nonspecific Lennard-Jones interactions (Fig. 1 *C*). On the other hand, if the binding domain is unmasked, it can form a specific bond with the ligand (Fig. 1 *D*). The lifetime of the ligand-receptor pair is calculated as follows: the interaction time starts when any of the dimer beads touches the ligand bead, and ends when both of the dimer beads leave the ligand bead. This time includes nonspecific and specific interactions.

Theory

To build a kinetic model, we first define the interacting domains as in state 1, when the masking domain is attached to the binding domain, and in state 2, when the masking domain is detached (Fig. 4 *A*). The rate constant from state 1 to state 2 follows the Bell mechanism (34) and can be written as

$$k_{12}(f) = k_{12}^0 \exp\left(\frac{r_0 f}{k_B T}\right), \quad (6)$$

where r_0 is the characteristic length of detachment, and k_{12}^0 is the rate constant from state 1 to state 2 without load. The value k_{12}^0 is related to the energy barrier for detaching the masking domain $E_{detach\ (mask)}$. The rate constant from state 2 to state 1 depends on the separation distance of the dimer R_{dimer}. Within the reaction distance $R_{reaction}$, the dimer tries to form bonds with rate constant k_{12}^0 (which is related to the energy barrier for attaching the masking domain $E_{attach\ (mask)}$), while the rate constant is zero when the dimer separation distance is larger than the reaction distance. It is assumed that the binding and the masking domain only interact within a specific distance, in which the two domains are very close to each other, and the interaction vanishes quickly when the dimers are apart, so that the step function approximation for the dimer reaction is used in the simulations.

The dimer distance R_{dimer} is a function of external force f. Solving $f = -dU_{FENE}/dR$, the force dependence of the equilibrium separation distance of the dimer is given by

$$R_{dimer}(f) = \frac{-\left(\frac{kR_0^2}{f}\right) + \sqrt{\left(\frac{kR_0^2}{f}\right)^2 + 4R_0^2}}{2}. \quad (7)$$

The distance dependence of the rate constant is drawn in Fig. 4 *B* and is approximated by a Fermi-Dirac-distribution-like function,

$$k_{21}(R_{dimer}(f)) = k_{21}^0\left\{\frac{1}{\exp[\alpha\cdot(R_{dimer}(f) - R_{reaction})] + 1}\right\}, \quad (8)$$

where α is a fitting constant that can be thought as the thermodynamic parameter that controls the shape of the function near the transition region when $R_{dimer} \sim R_{reaction}$. This particular approximate form arises from the fact that both molecules are bonded by a polymer chain. (We note that a more precise description could be formulated by calculating the probability distributions of the bond length of the dimer (35), but this is beyond the scope of this study.)

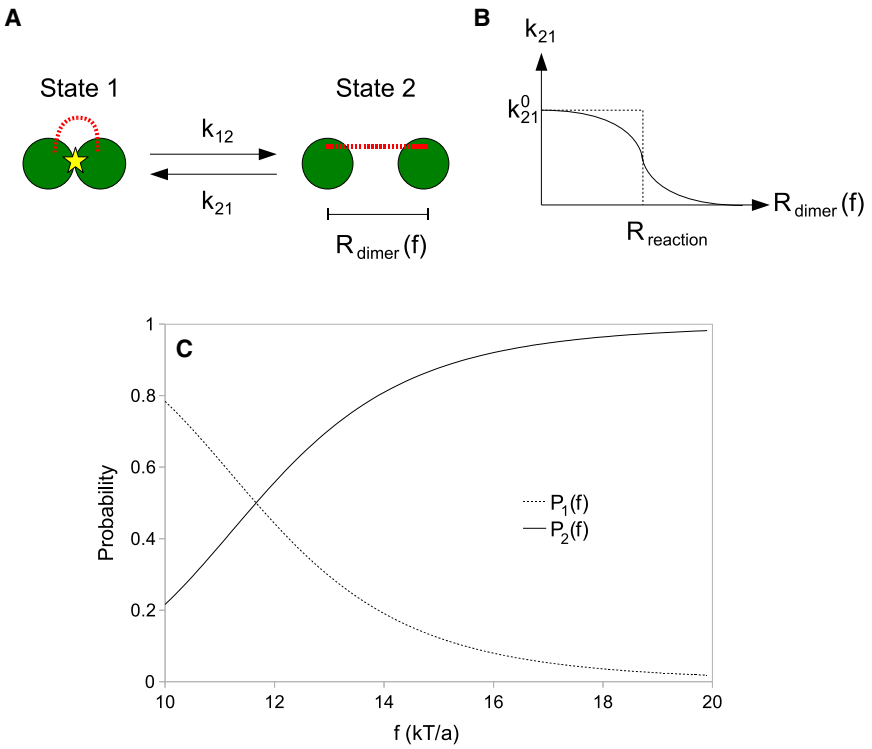

FIGURE 4 (*A*) Schematic of the two states of the dimer. (*B*) Distance dependence of the rate constant from state 2 to state 1. (Note that the *solid line* is the approximate function used in deriving the kinetic theory, and the *dotted line* is the step function used in stochastic simulations.) (*C*) Trends of the force dependence of the probabilities for the dimer to be in state 1 (P_1 (f)) and state 2 (P_2 (f)).

Assuming that the dimer reaches equilibration between the two states before encountering the ligand, the probabilities for the dimer to be in state 1 (P_1) and in state 2 (P_2) are

$$P_1(f) = \frac{k_{21}(R_{dimer}(f))}{k_{12}(f) + k_{21}(R_{dimer}(f))}, \quad P_2(f) = \frac{k_{12}(f)}{k_{12}(f) + k_{21}(R_{dimer}(f))}. \tag{9}$$

Fig. 4 *C* shows the trend of P_1 (f) and P_2 (f). As expected, the dimer is more probable to be in state 1 in the small-force regime, and it is more probable to be in state 2 in the large-force regime. When in state 1, the dimer only interacts with the ligand with nonspecific interactions which we assume to be characterized by the interaction time τ_1 as

$$\tau_1(f) = \tau_1^0 \exp\left(-\frac{r_1 f}{k_B T}\right), \tag{10}$$

where r_1 and τ_1^0 are to be fitted from the simulations.

When in state 2, the binding domain can form specific bonds with the ligand. The force-dependence of the bond lifetime $\tau_2(f)$ follows the Bell type form (34) and can be written as

$$\tau_2(f) = \tau_2^0 \exp\left(-\frac{r_2 f}{k_B T}\right), \tag{11}$$

where r_2 is the characteristic length for detaching the dimer from the ligand, and $\tau^0{}_2$ is the average bond lifetime with the absence of external force. We extract all the effective distances r_1 and r_2, as well as the characteristic times $\tau^0{}_1$ and $\tau^0{}_2$ from the simulations using the unmasked (for state 1) and masked case (for state 2). Finally, the time average interaction lifetime of the dimer and the ligand can be written as

$$\bar{\tau}(f) = P_1(f)\tau_1(f) + P_2(f)\tau_2(f), \tag{12}$$

where P_1 and P_2 are the weights for the two states. Equation 12 can be verified by the two extremes. When state 1 dominates, $P_1 \sim 1, P_2 \sim 0$, and $\bar{\tau} \sim \tau_1$. On the other hand, when state 2 dominates, $P_1 \sim 0$, $P_2 \sim 1$, and $\bar{\tau} \sim \tau_2$. In both cases, the interaction time is coincident with the bond lifetime of the dominate state.

RESULTS AND DISCUSSION

General catch-bond behavior

In the simulation, we apply an external force that ranges from $f = 10\ k_BT/a$ to $f = 20\ k_BT/a$ (which can be seen as applying different shear rates in the experimental flow chamber), and observe the bond lifetime sequentially, because the dimer is allowed to pass the binding site many times. The strength of the LJ potential is taken to be $\varepsilon = 10\ k_BT$. The characteristic length of detachment is set to be $r_0 = 0.1a$ for all specific bonds. All other simulation parameters, along with the parameters in the following sections, are summarized in Table 1.

Apart from the case in which we are interested here that corresponds to the dynamic masking case, which refers to the condition that the masking domain is free to interact with the binding domain through the attach-detach process described above, we also perform simulations in the unmasked case and masked case. Unmasked refers to the condition that the masking domain does not interact with the binding domain, and it is always detached. Masked, on the other hand, refers to the condition that the masking domain is always attached to the binding domain, and the dimer and the ligand can only interact with nonspecific interactions at all times. Last but not least, we do simulations in the no masking domain case, which refers to the condition that only the binding domain is simulated and the masking domain is removed. We use the no masking domain case to compare and understand whether the dimer structure affects the interaction lifetime.

The kinetic theory is applied as follows:

First, the force dependences of the interaction time for the two states (Eqs. 10 and 11) are fitted to the unmasked and the masked case, respectively. In essence, the dimer is always in state 1 in the masked regime, and always in state 2 in unmasked case.

Second, the FENE spring properties (k and R_0) are plugged into Eq. 7 to calculate the equilibrium dimer distance.

Third, the ratio of the rate constant of the dimer from state 1 to state 2 (in the absence of external force) and the rate constant from state 2 to state 1 should equal to

$$\frac{k_{12}^0}{k_{21}^0} = \frac{\exp\left(-E_{detach\ \ (mask)}\right)}{\exp\left(-E_{attach\ \ (mask)}\right)}, \tag{13}$$

which leaves us only with two undetermined constants, $R_{reaction}$ and α. We use these constants as fitting parameters for the data in the dynamic masking case. For the

TABLE 1 Summary of simulation parameters

Simulation condition	E_{attach} (k_BT)		E_{detach} (k_BT)		k (k_BT/a^2)	R_0 (a)	Result
	Mask	Ligand	Mask	Ligand			
Masked	∞	1	N/A	10	1	8	Fig. 5
Dynamic masking	1	1	10	10	1	8	Fig. 5
No masking domain	N/A	1	N/A	10	N/A	N/A	Fig. 5
Unmasked	N/A	N/A	∞	N/A	1	8	Fig. 5
Change detach energy (mask)	1	1	8 ~ 14	10	1	8	Fig. 7
Change detach energy (ligand)	1	1	10	6 ~ 12	1	8	Fig. 8
Change spring constant	1	1	10	10	0.8 ~ 2	8	Fig. 9 *A*
Change spring maximum bond length	1	1	10	10	1	4 ~ 14	Fig. 9 *B*

no-masking domain case, because there is no masking effect, we expect that the force dependence of the bond lifetime shows a monotonic decay, and it is fitted with the same equation as Eq. 11.

Fig. 5 shows typical results for the unmasked, masked, dynamic masking, and no-masking domain cases. As can be clearly seen, the dynamic masking condition leads to a bond lifetime that first increases when the applied external force increases, reaches a maximum at an external force of $f = 13–14\ k_BT/a$, and decreases afterwards when the external force is increased further. The catch-bond behavior of the dynamic masking case comes from the force-dependent competition between the two binding partners: the masking domain and the ligand in the surface. In the small-force regime, the masking domain is usually attached to the binding domain, hence the dimer and the ligand can only interact with short-lifetime, nonspecific interactions. When the external force increases, the probability of detaching the masking domain increases: more and longer lifetime specific ligand-receptor bonds can be formed, and the average bond lifetime increases. In the large force regime, the masking domain is mostly detached from the binding domain. The interaction of the dimer and the ligand is dominated by the specific ligand-receptor bond in this force regime; however, with very high external force, the lifetime of the specific ligand-receptor bond also decreases.

When no masking domain is present, the bond lifetime is smaller in all the force range. This is due to the fact that when the ligand interacts with the dimer, the ligand falls into the pocket between the binding domain and the masking domain. This pocket structure will not change during the whole protein-ligand interaction. With the assumption that the timescale of the polymer relaxation is much longer than the timescale of the protein-ligand interaction, the tailing end of the polymer will not have enough time to relax, or bend, downstream from the binding domain even if the binding domain forms a bond to the stationary ligand. As a result, the dimer should always be constrained. The two domains act as a clamp, making it harder for the ligand to escape. Removing the masking domain also removes this clamping effect.

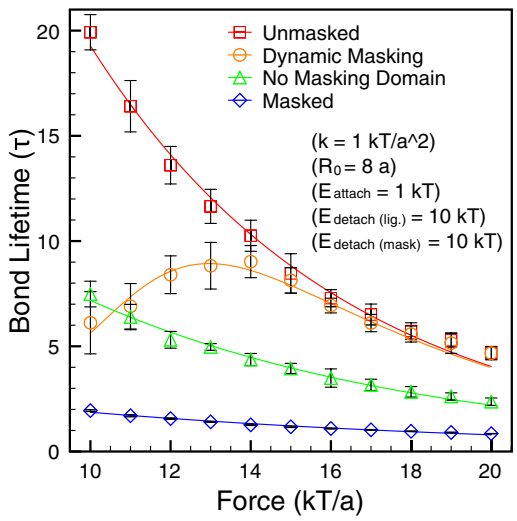

FIGURE 5 Plot of the bond lifetime versus force for unmasked, dynamic masking, no masking domain, and masked cases. (*Symbols* are from stochastic simulations, and *solid lines* are the corresponding curves from the kinetic theory. The simulation parameters used here are: $k = 1\ kT/a^2$, $R_0 = 8a$, $E_{attach} = 1\ kT$, $E_{detach\ (lig.)} = 10\ kT$, and $E_{detach\ (mask)} = 10\ kT$.)

Fig. 6 shows the detaching routes of the ligand from the dimer structure or from a monomer. As can be seen, in the dimer structure, the ligand has to bypass the masking domain to be successfully detached, although it is much simpler for the ligand to leave a monomer. Of course, the properties of the linker chain modulate this behavior, as is shown below. The fitted characteristic length of detachment (using Eq. 11) for the unmasked case is $r_0 \sim 0.17a$, which is larger than the input characteristic length of detachment of the ligand-binding domain bond ($r_{0\ (input)} = 0.1a$). This may reflect the fact that the ligand has to go through a longer path to be detached from the dimer structure. On the other hand, the fitted characteristic length of detachment for the remove masking domain case is $r_0 \sim 0.12a$, which is very close to the input characteristic length of the ligand-binding domain bond, as expected.

Effect of energy barriers

Fig. 7 shows different force dependences of the bond lifetime when the energy barriers for detaching the masking domain are changed. When the energy barrier for detaching the masking domain is small, it is easier for the masking

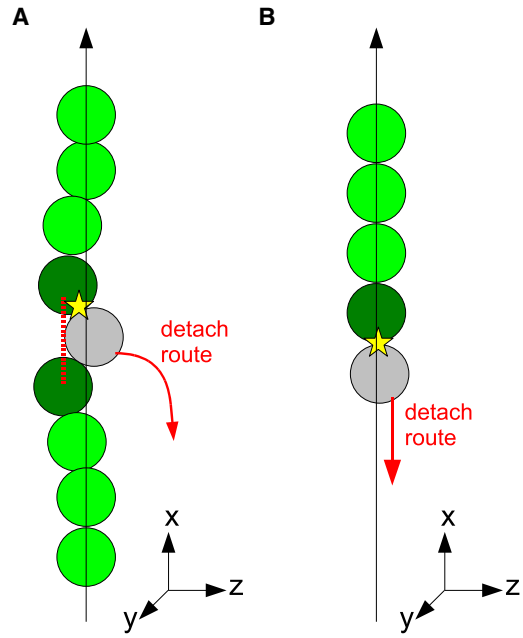

FIGURE 6 Schematic of the detach routes of the ligand from a dimer (*A*) and a monomer (*B*).

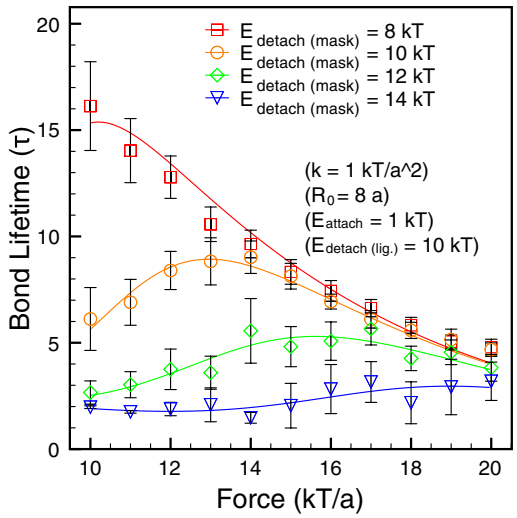

FIGURE 7 Force dependence of the bond lifetime when changing the energy barrier for detaching the masking domain. The different barriers are shown in the figure. (*Symbols* are from stochastic simulations, and *solid lines* are the corresponding curves from the kinetic theory. The simulation parameters used here are: $k = 1\ kT/a^2$, $R_0 = 8a$, $E_{attach} = 1\ kT$, $E_{detach\ (lig\cdot)} = 10\ kT$, and $E_{detach\ (mask)} = 8 \sim 10\ kT$.)

domain to be detached, and thus it is more probable for the binding domain to form a specific bond with the ligand. In the kinetic model, one can derive in a straightforward fashion that the probability for the dimer to be in state 2 is higher when the energy barrier for detaching the masking domain is smaller.

When $E_{detach\ (mask)} = 8\ k_BT$, the masking effect is not obvious in the force regime studied, and the force dependence of the bond lifetime is similar to the unmasked case. (However, it is suspected that the $E_{detach\ (mask)} = 8\ k_BT$ case is actually a catch-bond with a bond lifetime that peaks at $f = 10\ k_BT/a$, whereas the unmasked case has a much longer lifetime below that value.) On the other hand, when the energy barrier for detaching the masking domain equals 14 k_BT, the masking domain is not easily detached from the binding domain, and the dimer and ligand interact with each other, mostly with short lifetime nonspecific interactions unless a very high external force is applied.

Fig. 8 shows different force dependences of the bond lifetime when we change the energy barrier for detaching the ligand from the binding domain, while keeping the energy barrier for detaching the masking domain unchanged. Because the force dependences of the bond lifetime in state 2 (Eq. 11) are different with different energy barriers for detaching the ligand, we also perform simulations for the unmasked case under these conditions. It can be seen from Fig. 8 *A* that the overall bond lifetime changes dramatically when changing the energy barrier for detaching the ligand. This is because the bond lifetime of state 2 (in the absence of external force) depends exponentially on the energy barrier for detaching the ligand (34),

$$\tau_2^0 \sim \exp\left(E_{detach\ \ (lig.)}\right). \tag{14}$$

Fig. 8 *B* shows the force dependences of the bond lifetime in a normalized axis. As can be seen on the figure, the profiles of the force dependence of the bond lifetime are very similar. Although the energy barriers for detaching the ligand are different, the energy barrier for detaching the masking domain is the same, and the attach-detach dynamics of the masking domain is not affected. The probabilities for the dimer to be in state 1 and state 2 are the same as long as the energy barrier for detaching the masking domain and the properties of the spring connecting the two domains are the same.

To summarize the effects of the energy barriers, we find that the energy barriers for detaching the masking domain and the ligand affect the force dependence on the bond lifetime in very different ways. Observing the occurrence of the maximum bond lifetime in both cases, one finds that the range of forces at which the maximum lifetime occurs is much larger when we vary $E_{detach\ (mask)} = 8 - 14\ k_BT$, where we find that the peak lifetime occurs in the range of $f \sim 10\text{–}18\ k_BT/a$.

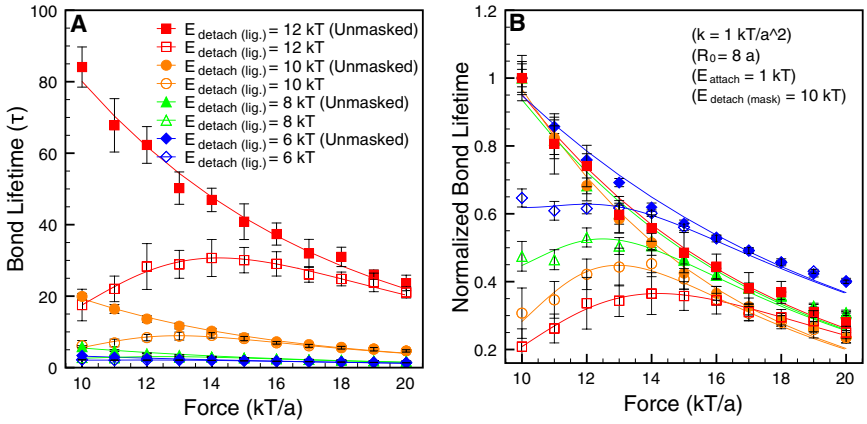

FIGURE 8 (*A*) Force dependence of the bond lifetime when changing the energy barrier for detaching the ligand. (*B*) For clarity, the data in panel *A* is normalized by dividing by the maximum bond lifetime from the unmasked case. (*Symbols* are from stochastic simulations, and *solid lines* are the corresponding curves from the kinetic theory. The simulation parameters used here are: $k = 1\ kT/a^2$, $R_0 = 8a$, $E_{attach} = 1\ kT$, $E_{detach\ (lig\cdot)} = 6 \sim 12\ kT$, and $E_{detach\ (mask)} = 10\ kT$.)

Meanwhile, it occurs in a much smaller range $f \sim 12$–$14\ k_BT/a$ when $E_{detach\ (lig.)} = 6 - 12\ k_BT$. On the other hand, the maximum bond-lifetime in both cases also differs considerably. The maximum bond lifetime decreases from 15τ to 3τ when increasing $E_{detach\ (mask)}$ from 8 k_BT to 14 k_BT, while the maximum lifetime increases rapidly from 2τ to 30τ when increasing $E_{detach\ (lig.)}$ from 6 k_BT to 12 k_BT.

Effects of properties of the polypeptide chain connecting the two domains

To observe the effects of the properties of the polypeptide chain connecting two domains, we change the spring constant and maximum extension of the FENE spring. Fig. 9 *A* presents the effects of the spring constant of the FENE spring. As can be seen, the larger the spring constant, the more the bond lifetime decreases in the whole force range, and the maximum bond lifetime shifts closer to a high-force regime. From the kinetic theory, it is more probable for the dimer to be in state 1 with a larger spring constant, and the masking effect increases with a larger spring constant. Fig. 9 *B* shows the effects of the maximum bond length. The profiles of the bond lifetime are very similar when $R_0 \geq 8a$. The force dependence of the bond lifetime changes manifest themselves in the small force regime, while the curves overlap in high force regime. The masking effect is less obvious when the maximum bond length increases. On the other hand, when the maximum bond length is very small ($R_0 = 4a$), the bond lifetime is very small for all the force range considered here, very similar to the masked case.

In sum, the properties of the connecting chain strongly modulate the catch-bond behavior. The longer the maximum bond length and the smaller the spring constant, the farther the binding and the masking domain will be when detached, and the masking effect that much less effective. While the spring constant and the maximum bond length both influence the masking effect, the masking effect is more sensitive to the spring constant. Also note from the fitting curves that our kinetic theory faithfully captures this behavior.

CONCLUSIONS

In this work we have demonstrated that (bio) polymers with interacting domains can display catch-bond characteristics. Simulation results were compared with kinetic theory and the agreement was very good. The effects of the energy barriers for detaching the domains and the ligand, and of the properties of the FENE spring connecting domains, were shown to play a key role in the binding behavior. We want to point out that the parameters used in our simulation can be linked to the real world.

In general, $k_BT \sim 4.4$ pN•nm. For typical protein domains with radius $a \sim 5$ nm, the force range, $f = 10 - 20\,k_BT/a \sim 8.8 - 17.6$ pN, is inside the biologically relevant range where the catch-bonds are found experimentally (3,4,6,7). In a typical environment, the fluid viscosity is $\eta \sim 10^{-3}$ Pa•s, and the characteristic diffusion time is $\tau \sim 5.4\times10^{-4}$ms. The energy barrier for detaching the ligand is $E_{detach\ (lig.)} \sim 10\,k_BT$, and the bond lifetime is approximately $t_{lifetime} = 5$–$30\,\tau \sim 0.0027 - 0.0162$ ms.

The lifetime may be shorter in magnitude when compared to the experiment data; however, the lifetime can increase dramatically when we slightly adjust the energy barrier of detachment. For example, in Fig. 8 *A*, the maximum bond lifetime (without masking effect) increases fourfold from 20τ to $>80\tau$ when we change $E_{detach\ (lig.)}$ from 10 k_BT to 12 k_BT.

Furthermore, we can also relate to the conditions necessary to unfold globular multimeric proteins, such as vWF. In this case, we would estimate the tension force along the backbone to be of $\sim 6\pi\eta\dot{\gamma}\sin\theta L^2$, where L is the length of the stretched protein, η the viscosity, $\dot{\gamma}$ the shear rate, and θ the tilt angle when unraveling.

Under the conditions in which vWF operates, one would have $\dot{\gamma} \sim 10^3, L \sim 1\ \mu$m, and $\eta \sim 10^{-3}$ Pa•s, which yield an estimated tension force of ~20 pN, which clearly agrees with the results presented above, as well as with the biologically relevant regime. We must mention that it has recently been found that catch-bonds form between the vWF A1

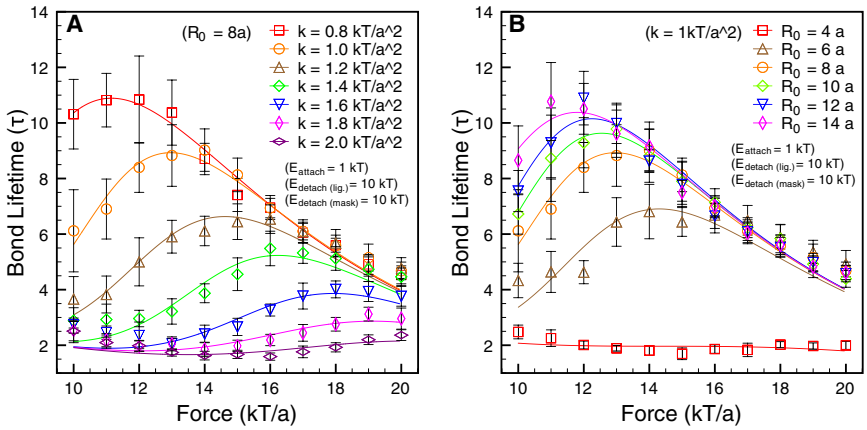

FIGURE 9 (*A*) Plot of bond lifetime versus force with different spring constants of the FENE spring, and (*B*) different maximum bond lengths of the FENE spring. (*Symbols* are from stochastic simulations, and *solid lines* are the corresponding curves from the kinetic theory. The simulation parameters used here are: $k = 0.8 \sim 2\ kT/a^2$, $R_0 = 4 \sim 14a$, $E_{attach} = 1\ kT$, $E_{detach\ (lig.)} = 10\ kT$, and $E_{detach\ (mask)} = 10\ kT$.)

domain and platelet GPIb domain, and the forces they encounter are similar to those found in this study (6). However, they cannot explain the observed masking effect of increasing the concentration of the A2 domain in the solution (25). We believe our model may help in relating both effects—explaining the role of A2 masking as well as the observed catch-bond behavior of vWF.

Catch-bonds also have important engineering applications because they lead to reinforcement as stress is applied. Some possible applications based on specific catch-bond receptor-ligand pairs have been put forward previously. Forero et al. (36) have developed a catch-bond based nanoadhesive which is sensitive to shear stress and binds strongly only within a characteristic force range. In fact, artificial catch-bond like behavior has been used in the assembly of hybrid nanostructure systems (37).

The polymer catch-bond mechanism proposed in this article is a general model that contributes to the different design strategies for synthesizing artificial catch-bonds. We also believe that this proposed mechanism will be important in understanding naturally occurring catch-bond behavior in the multimeric proteins that constitute a large portion of the extracellular matrix.

The authors thank Carsten Baldauf for inspiring conversations and the DuPont-MIT Alliance (DMA) for funding.

REFERENCES

1. Sokurenko, E. V., V. Vogel, and W. E. Thomas. 2008. Catch-bond mechanism of force-enhanced adhesion: counterintuitive, elusive, but … widespread? *Cell Host Microbe.* 4:314–323.
2. Thomas, W. E., E. Trintchina, …, E. V. Sokurenko. 2002. Bacterial adhesion to target cells enhanced by shear force. *Cell.* 109:913–923.
3. Marshall, B. T., M. Long, …, C. Zhu. 2003. Direct observation of catch bonds involving cell-adhesion molecules. *Nature.* 423:190–193.
4. Sarangapani, K. K., T. Yago, …, C. Zhu. 2004. Low force decelerates L-selectin dissociation from P-selectin glycoprotein ligand-1 and endoglycan. *J. Biol. Chem.* 279:2291–2298.
5. Guo, B., and W. H. Guilford. 2006. Mechanics of actomyosin bonds in different nucleotide states are tuned to muscle contraction. *Proc. Natl. Acad. Sci. USA.* 103:9844–9849.
6. Yago, T., J. Lou, …, C. Zhu. 2008. Platelet glycoprotein Ibα forms catch bonds with human WT vWF but not with type 2B von Willebrand disease vWF. *J. Clin. Invest.* 118:3195–3207.
7. Kong, F., A. J. García, …, C. Zhu. 2009. Demonstration of catch bonds between an integrin and its ligand. *J. Cell Biol.* 185:1275–1284.
8. Lou, J., T. Yago, …, R. P. McEver. 2006. Flow-enhanced adhesion regulated by a selectin interdomain hinge. *J. Cell Biol.* 174:1107–1117.
9. Aprikian, P., V. Tchesnokova, …, E. Sokurenko. 2007. Interdomain interaction in the FimH adhesin of *Escherichia coli* regulates the affinity to mannose. *J. Biol. Chem.* 282:23437–23446.
10. Tchesnokova, V., P. Aprikian, …, E. Sokurenko. 2008. Integrin-like allosteric properties of the catch bond-forming FimH adhesin of *Escherichia coli*. *J. Biol. Chem.* 283:7823–7833.
11. Yakovenko, O., S. Sharma, …, W. E. Thomas. 2008. FimH forms catch bonds that are enhanced by mechanical force due to allosteric regulation. *J. Biol. Chem.* 283:11596–11605.
12. Lou, J., and C. Zhu. 2007. A structure-based sliding-rebinding mechanism for catch bonds. *Biophys. J.* 92:1471–1485.
13. Gunnerson, K. N., Y. V. Pereverzev, and O. V. Prezhdo. 2009. Atomistic simulation combined with analytic theory to study the response of the P-selectin/PSGL-1 complex to an external force. *J. Phys. Chem. B.* 113:2090–2100.
14. Evans, E., A. Leung, …, C. Zhu. 2004. Mechanical switching and coupling between two dissociation pathways in a P-selectin adhesion bond. *Proc. Natl. Acad. Sci. USA.* 101:11281–11286.
15. Barsegov, V., and D. Thirumalai. 2005. Dynamics of unbinding of cell adhesion molecules: transition from catch to slip bonds. *Proc. Natl. Acad. Sci. USA.* 102:1835–1839.
16. Zhu, C., J. Lou, and R. P. McEver. 2005. Catch bonds: physical models, structural bases, biological function and rheological relevance. *Biorheology.* 42:443–462.
17. Pereverzev, Y. V., O. V. Prezhdo, …, W. E. Thomas. 2005. The two-pathway model for the catch-slip transition in biological adhesion. *Biophys. J.* 89:1446–1454.
18. Thomas, W., M. Forero, …, V. Vogel. 2006. Catch-bond model derived from allostery explains force-activated bacterial adhesion. *Biophys. J.* 90:753–764.
19. Pereverzev, Y. V., and O. V. Prezhdo. 2006. Force-induced deformations and stability of biological bonds. *Phys. Rev. E.* 73:050902.
20. Pereverzev, Y. V., O. V. Prezhdo, and E. V. Sokurenko. 2009. Allosteric role of the large-scale domain opening in biological catch-binding. *Phys. Rev. E.* 79:051913.
21. Liu, F., Z. C. Ou-Yang, and M. Iwamoto. 2006. Dynamic disorder in receptor-ligand forced dissociation experiments. *Phys. Rev. E.* 73:010901.
22. Liu, F., and Z. C. Ou-Yang. 2006. Force modulating dynamic disorder: a physical model of catch-slip bond transitions in receptor-ligand forced dissociation experiments. *Phys. Rev. E.* 74:051904.
23. Wei, Y. 2008. Entropic-elasticity-controlled dissociation and energetic-elasticity-controlled rupture induce catch-to-slip bonds in cell-adhesion molecules. *Phys. Rev. E.* 77:031910.
24. Sadler, J. E. 1998. Biochemistry and genetics of von Willebrand factor. *Annu. Rev. Biochem.* 67:395–424.
25. Martin, C., L. D. Morales, and M. A. Cruz. 2007. Purified A2 domain of von Willebrand factor binds to the active conformation of von Willebrand factor and blocks the interaction with platelet glycoprotein Ibα. *J. Thromb. Haemost.* 5:1363–1370.
26. Warner, H. R. 1972. Kinetic-theory and rheology of dilute suspensions of finitely extendible dumbbells. *Ind. Eng. Chem. Fundam.* 11:379–387.
27. Marko, J. F., and E. D. Siggia. 1994. Fluctuations and supercoiling of DNA. *Science.* 265:506–508.
28. Somasi, M., B. Khomami, …, E. S. G. Shaqfeh. 2002. Brownian dynamics simulations of bead-rod and bead-spring chains: numerical algorithms and coarse-graining issues. *J. Non-Newt. Fluid Mech.* 108:227–255.
29. Underhill, P. T., and P. S. Doyle. 2004. On the coarse-graining of polymers into bead-spring chains. *J. Non-Newt. Fluid Mech.* 122:3–31.
30. De Gennes, P. G. 1974. Coil-stretch transition of dilute flexible polymers under ultrahigh velocity-gradients. *J. Chem. Phys.* 60:5030–5042.
31. Smith, D. E., H. P. Babcock, and S. Chu. 1999. Single-polymer dynamics in steady shear flow. *Science.* 283:1724–1727.
32. Larson, R. G. 2005. The rheology of dilute solutions of flexible polymers: progress and problems. *J. Rheol. (NY).* 49:1–70.
33. Alexander-Katz, A., M. F. Schneider, …, R. R. Netz. 2006. Shear-flow-induced unfolding of polymeric globules. *Phys. Rev. Lett.* 97:138101.
34. Bell, G. I. 1978. Models for the specific adhesion of cells to cells. *Science.* 200:618–627.
35. Moreira, A. G., and C. M. Marques. 2004. The role of polymer spacers in specific adhesion. *J. Chem. Phys.* 120:6229–6237.
36. Forero, M., W. E. Thomas, …, V. Vogel. 2004. A catch-bond based nanoadhesive sensitive to shear stress. *Nano Lett.* 4:1593–1597.
37. Agarwal, A., P. Katira, and H. Hess. 2009. Millisecond curing time of a molecular adhesive causes velocity-dependent cargo-loading of molecular shuttles. *Nano Lett.* 9:1170–1175.